Radiotherapy and Oncology 184 (2023) 109675

Contents lists available at ScienceDirect

Radiotherapy and Oncology

journal homepage: www.thegreenjournal.com

Original Article

Consensus guide on CT-based prediction of stopping-power ratio using a Hounsfield look-up table for proton therapy

Nils Peters [a,b,1,*], Vicki Trier Taasti [c,1,*], Benjamin Ackermann [d,2], Alessandra Bolsi [e,2], Christina Vallhagen Dahlgren [f,2], Malte Ellerbrock [d,2], Francesco Fracchiolla [g,2], Carles Gomà [h,2], Joanna Góra [i,2], Patricia Cambraia Lopes [j,2], Ilaria Rinaldi [c,2], Koen Salvo [k,2], Ivanka Sojat Tarp [l,2], Alessandro Vai [m,2], Thomas Bortfeld [b], Antony Lomax [e], Christian Richter [a,n,o,p], Patrick Wohlfahrt [b,3]

[a] OncoRay – National Center for Radiation Research in Oncology, Faculty of Medicine and University Hospital Carl Gustav Carus, Technische Universität Dresden, Helmholtz-Zentrum Dresden - Rossendorf, Germany; [b] Massachusetts General Hospital and Harvard Medical School, Department of Radiation Oncology, Boston, MA, USA; [c] Department of Radiation Oncology (Maastro), GROW School for Oncology and Reproduction, Maastricht University Medical Centre+, Maastricht, The Netherlands; [d] Heidelberg Ion-Beam Therapy Center (HIT), Department of Radiation Oncology, Heidelberg University Hospital, Heidelberg, Germany; [e] Center for Proton Therapy, Paul Scherrer Institute, Villigen, Switzerland; [f] The Skandion Clinic, Uppsala, Sweden; [g] Azienda Provinciale per i Servizi Sanitari (APSS) Protontherapy Department, Trento, Italy; [h] Department of Radiation Oncology, Hospital Clínic de Barcelona, Barcelona, Spain; [i] MedAustron Ion Therapy Center, Wiener Neustadt, Austria; [j] HollandPTC, Delft, the Netherlands; [k] AZ Sint-Maarten, Department of Radiotherapy, Mechelen, Belgium; [l] Aarhus University Hospital, Danish Center for Particle Therapy, Aarhus, Denmark; [m] Radiotherapy Department, Center for National Oncological Hadrontherapy (CNAO), 27100 Pavia, Italy; [n] Helmholtz-Zentrum Dresden – Rossendorf, Institute of Radiooncology – OncoRay; [o] Department of Radiotherapy and Radiation Oncology, Faculty of Medicine and University Hospital Carl Gustav Carus, Technische Universität Dresden, Dresden; and [p] German Cancer Consortium (DKTK), partner site Dresden, and German Cancer Research Center (DKFZ), Heidelberg, Germany

ARTICLE INFO

Article history:
Received 22 December 2022
Received in revised form 8 March 2023
Accepted 10 April 2023
Available online 19 April 2023

Keywords:
Hounsfield look-up table
Proton therapy
Single-energy CT
Stoichiometric calibration
Stopping-power ratio
Proton range prediction

ABSTRACT

Background and purpose: Studies have shown large variations in stopping-power ratio (SPR) prediction from computed tomography (CT) across European proton centres. To standardise this process, a step-by-step guide on specifying a Hounsfield look-up table (HLUT) is presented here.

Materials and methods: The HLUT specification process is divided into six steps: Phantom setup, CT acquisition, CT number extraction, SPR determination, HLUT specification, and HLUT validation. Appropriate CT phantoms have a head- and body-sized part, with tissue-equivalent inserts in regard to X-ray and proton interactions. CT numbers are extracted from a region-of-interest covering the inner 70% of each insert in-plane and several axial CT slices in scan direction. For optimal HLUT specification, the SPR of phantom inserts is measured in a proton beam and the SPR of tabulated human tissues is computed stoichiometrically at 100 MeV. Including both phantom inserts and tabulated human tissues increases HLUT stability. Piecewise linear regressions are performed between CT numbers and SPRs for four tissue groups (lung, adipose, soft tissue, and bone) and then connected with straight lines. Finally, a thorough but simple validation is performed.

Results: The best practices and individual challenges are explained comprehensively for each step. A well-defined strategy for specifying the connection points between the individual line segments of the HLUT is presented. The guide was tested exemplarily on three CT scanners from different vendors, proving its feasibility.

Conclusion: The presented step-by-step guide for CT-based HLUT specification with recommendations and examples can contribute to reduce inter-centre variations in SPR prediction.

Range prediction in proton and ion treatment planning is commonly based on an X-ray computed tomography (CT) scan of the patient. In the following, we refer to protons only without loss of generality. Since X-rays interact differently with tissue than protons, the stopping-power ratio (SPR) used for proton dose calculation cannot be directly obtained from CT scans. Instead, CT numbers need to be translated into SPR using a heuristic conversion, a so-called Hounsfield look-up table (HLUT). This translation is ambiguous, since tissues can have similar CT numbers but

* Corresponding author at: Nils Peters: Massachusetts General Hospital, Department of Radiation Oncology, 100 Blossom Street, Boston, MA 02114, United States of America. Vicki Trier Taasti: Maastro Clinic, Doctor Tanslaan 12, 6229 ET Maastricht, The Netherlands

E-mail addresses: nilspetersmp@gmail.com (N. Peters), vicki.taasti@maastro.nl (V. Trier Taasti).

[1] Both authors, listed alphabetically, share first authorship.

[2] Co-authors are listed in alphabetical order.

[3] Now with Siemens Healthineers, Forchheim, Germany.

https://doi.org/10.1016/j.radonc.2023.109675
0167-8140/

different SPRs [1]. The uncertainty in the HLUT specification is one of the main contributing factors to proton range uncertainty [2].

For HLUT specification, material-specific CT numbers and SPRs are obtained by measurements of phantom inserts [3] or stoichiometric calculation of tabulated human tissues [4]. A piecewise linear fit of pairs of CT numbers and SPRs is performed to improve the HLUT stability compared to a simple connection of the datapoints [5]. As CT numbers depend on the X-ray spectrum of the specific CT scanner as well as scan and reconstruction settings, a direct comparison or adoption of HLUTs by different proton centres is not feasible. Consequently, the HLUT is defined by each proton centre and for each CT scanner individually. Moreover, several factors influence the HLUT specification, for example the experimental setup used for calibration, the selection of phantom inserts and the fitting procedure. Each choice in the calibration process can affect the accuracy in proton range prediction and varies greatly between proton centres [6].

In an experimental study conducted within the European Particle Therapy Network (EPTN), a variation in range prediction of about 3% of beam range was observed [7]. This variation is on the level of the range uncertainty margin applied by most clinics [6]. In the EPTN study, potential error sources, such as the calibration method, the consideration of beam hardening, and the used validation framework were assessed. The latter two showed the biggest potential for improvement [7].

Several aspects of the calibration procedure have been discussed in the proton therapy community, but so far, no consensus exists. In this work, a comprehensive guide is presented, describing all relevant steps for HLUT specification, starting from phantom setups via CT scan acquisition, SPR determination, HLUT specification, and finally ending with suggestions for an appropriate HLUT evaluation. Recommendations along with their rationale are provided for each step according to literature and based on additional analyses performed in this work. This step-by-step guide was created within the European Society for Radiotherapy and Oncology (ESTRO) Physics Workshop 2021 in a joint effort with the EPTN Work Package 5 (WP5). It thereby represents a consensus found within the European proton therapy community. The guide aims at both the improvement of treatment quality in individual centres by reducing range prediction inaccuracies and a better data comparability by decreasing the range prediction variability between centres.

In the following, the guide is briefly summarised by highlighting novel aspects and its clinical applicability. To illustrate its feasibility, HLUT specifications have been exemplarily performed for CT scanners from three vendors, covering both conventional single-energy CT (SECT) and virtual monoenergetic images (VMIs) derived from dual-energy CT (DECT). The comprehensive step-by-step guide, comprising a detailed description of all aspects along with their rationale and illustrative examples, is provided in Supplement S1.

Material and methods

The HLUT specification consists of six steps, covering all relevant aspects in the calibration process. Furthermore, each step is implemented in programming code (Python and Matlab) supplied in a GitHub repository: https://github.com/CTinRT/HLUT-guide.

Step 1: Phantom setup

Appropriate calibration phantoms simulate X-ray beam hardening conditions comparable to patient scenarios, e.g. a small cylindrical phantom for head or paediatric cases and a large ellipsoidal phantom for abdomen or pelvis, resulting in the need for multiple phantom sizes. Well-suited phantom inserts mimic tabulated human tissues in their elemental composition [8], i.e. they are tissue-equivalent for both X-ray and proton interactions. Considering multiple phantom inserts in each tissue group, i.e. lung, adipose, soft and bone tissues, improves the calibration stability. Since the arrangement of multiple bone phantom inserts in a single setup can introduce artefacts, separate CT scans for each bone insert are recommended.

Step 2: CT scan acquisition and reconstruction settings

Material-specific CT numbers are used to characterise the X-ray energy spectrum of the CT scanner. This characterisation allows for an estimation of scanner-specific CT numbers of tabulated human tissues (see details in Supplement S3). Hence, tabulated human tissues can be included together with phantom inserts in the HLUT specification.

Some CT scan and reconstruction parameters have an impact on CT numbers, such as tube voltage, detector collimation, choice of reconstruction kernel, and applied beam hardening correction [9]. Consequently, the CT scan settings used for HLUT specification need to be consistent with the clinically applied CT scan protocols. A reconstruction kernel with a soft image impression, an iterative image reconstruction for noise reduction, and a beam hardening correction for dense materials like bones is recommended.

When different CT scanner models, tube voltages, or scan protocols are used in clinical routine, individual HLUTs need to be generated for each of them to account for potential CT number differences. The CT scan protocol to be used for patient scanning should therefore be settled before performing phantom scans for HLUT specification. Scans obtained with an extended field-of-view (FOV) option, where CT number stability is not ensured outside the standard FOV [10], are not suitable for HLUT specification.

Step 3: CT number extraction

The mean CT number for each phantom insert is extracted from a cylindrical volume-of-interest (VOI). Artefacts from density gradients between the insert and the surrounding phantom can be avoided by limiting the VOI diameter to cover approximately 70% of the insert diameter in each axial CT slice. Moreover, including multiple axial CT slices from the centre of the phantom in the VOI increases statistics and minimises the influence of potential manufacturing heterogeneities in the inserts. However, CT slices close to phantom borders can be affected by edge artefacts due to missing forward scatter and are therefore excluded from the analysis. It is recommended to analyse line profiles, both in-plane and along the scan direction, to verify CT number stability in the phantom and inserts.

Step 4: Determination of stopping-power ratio

Including both phantom inserts and tabulated human tissues in the HLUT specification increases the calibration stability compared to just using one of the two datasets. Here, a subset of the tabulated human tissues collected by Woodard and White [8] was selected considering their occurrence in typical treatment scenarios (Table S1.3 in Supplement). SPR calculation for the tabulated human tissues follows the Bethe equation in combination with the mean excitation energies listed in ICRU report 49 [11] (Eq. (S3.1) and Table S1.6 in Supplement). The influence of the SPR energy dependency is minimised by applying a nominal beam energy of 100 MeV in the calculation [12].

The SPR of the phantom inserts can be determined either experimentally or computed via the Bethe equation. The highest accuracy can be achieved experimentally via proton spot

measurements through the inserts or material slabs from the same production batch. For computed SPRs, potential deviations in the chemical composition and density provided for the phantom inserts may diminish the SPR accuracy.

Step 5: HLUT specification

The HLUT is specified as a piecewise linear regression between CT numbers and SPRs for the phantom inserts and tabulated human tissues. The linear regression is performed individually for the four different tissue groups (lung, adipose, soft tissue, and bone). Since lung tissues have a composition comparable to soft tissues [8], they can be treated as low-density soft tissues and included in the regression fit of soft tissues. As CT numbers of the adipose and soft tissue datapoints as well as soft tissue and bone datapoints overlap, the attribution of a CT number interval to the respective fit is nontrivial. Here, observations made in DECT-derived frequency distributions of CT number and SPR pairs have been utilised to specify the CT number intervals for the line segment for each tissue group [1]. The individual line segments are connected with straight lines (Fig. 1). A detailed description including considerations on the placements of the connection points is provided in Supplement S1.

The HLUT is specified for each phantom size individually. By comparing the body-site-specific HLUTs (using CT numbers for the head and body phantom geometry, respectively) with a HLUT based on CT numbers averaged over the two sizes, the need for body-site-specific HLUTs can be evaluated.

Step 6: Evaluation of HLUT specification

By validating each step of the HLUT specification process, implementation errors can be prevented [7]. Necessary evaluations are highlighted for each step in Supplement S1. Recommended evaluations can be performed with the same phantom as used for HLUT specification.

CT number stability regarding beam hardening can be assessed by varying the phantom size (head/abdomen) and insert positions, especially for the bone inserts. The accuracy of each HLUT can be checked by comparing the SPR predicted using the HLUT with the reference SPR for the phantom inserts and tabulated human tissues.

Additional optional verification steps can be performed using a different electron density phantom fulfilling the recommendations of Step 1 as well as anthropomorphic phantoms or biological tissues to better mimic patient scenarios. The benefit of such additional verifications needs to be weighed against the potentially large experimental uncertainties in these complex validation scenarios.

Results

Following the detailed step-by-step guide described in Supplement S1, exemplary HLUTs were generated based on the Gammex Advanced Electron Density phantom (Sun Nuclear – A Mirion Medical Company, Middleton, WI, USA) for three different CT scanners: a GE Revolution CT (GE HealthCare, Milwaukee, WI, USA), a Philips Spectral CT 7500 (Philips Healthcare, Best, The Netherlands), and a Siemens SOMATOM go.Open Pro (Siemens Healthineers, Forchheim, Germany). For all three CT scanners, a 120 kVp X-ray spectrum was used. Since the Philips CT scanner used in this study contained a dual-layer detector with DECT capability, a VMI at 70 keV was generated to demonstrate that the step-by-step guide can be equally well applied on VMIs and conventional SECT images. The scan and reconstruction parameters are listed in Table 1. The respective CT numbers of the phantom inserts are included in the code in the Github repository https://github.com/CTinRT/HLUT-guide. The calculated SPRs for the tabulated human tissues are given in Table S1.6 in the Supplement.

The resulting HLUTs are shown in Fig. 2. Two HLUTs were calibrated for each CT scanner, one for the head-sized (blue) and one for the body-sized part of the phantom (green). For the scan protocols used on the GE and Philips CT scanners, the size dependency of the CT numbers was minor, resulting in almost identical HLUTs for the two phantom sizes. SPR deviations of the phantom inserts and tabulated human tissues are shown for both body-site-specific HLUTs as well as an HLUT based on the average CT numbers.

Discussion

A step-by-step guide on how to generate a HLUT for CT-based SPR prediction in proton treatment planning has been presented. It covers all relevant aspects required for HLUT specification and represents a consensus found within the European particle therapy community. This collective effort is an outcome of the 2021 ESTRO Physics Workshop in close collaboration with the EPTN WP5.

The uncertainty in proton range prediction is a major limiting factor in proton treatment planning. It hampers an optimal dose sparing of organs-at-risk [13,14] as well as the prediction of the biological effectiveness of protons [15]. The large variation in HLUT-based range prediction observed in a previous study stresses the need for a common standard [7]. The main issues identified – insufficient consideration of X-ray beam hardening and the lack of a dedicated HLUT validation procedure – were addressed here. The presented evaluation steps concern all parts of the HLUT specification procedure.

An analysis on the influence of different scan and calibration settings was described in the work of Ainsley and Yeager [16]. Furthermore, individual aspects of the recommendations presented in this step-by-step guide were already addressed in different publications, such as the large influence of the phantom size [9,17], the phantom insert choice for calibration [18], the influence of tissue composition [5], the impact of the reconstruction kernel [19] and the SPR energy dependence [12]. Here, they were embedded into a comprehensive description of the underlying analysis in a clinically feasible setup and supplemented with additional analysis and explanations of potential pitfalls in the respective steps.

A set of tabulated human tissues relevant for radiotherapy was selected from the extensive collection by Woodard and White [8] to ensure an equal contribution of the relevant tissues. Special attention was paid to the non-trivial implementation of the HLUT specification procedure itself (Step 5), which includes linear regression fitting in different tissue groups and the definition of the respective CT number intervals. For the latter, DECT-obtained body-region-specific tissue SPR distributions [1] were utilised. This utilisation of patient-specific SPR information expands the tissue region definition beyond an evaluation based purely on the CT number distribution seen in patients, as e.g. performed by Schaffner and Pedroni [20], and thus allows for a better description of the SPR in CT number regions where different tissue types overlap. Lastly, validation, both after each step of the procedure and in an overall end-to-end test, was emphasised as a mandatory step in the HLUT specification.

The presented step-by-step guide is applicable to all commercially available CT scanners, both on SECT images and DECT-derived VMIs. The resulting HLUT can be used in all major treatment planning systems (TPSs). Some TPSs might require a HLUT to predict mass density (MD) from CT numbers instead of SPR as described here. The considerations presented here also apply to the creation of an MD HLUT. However, the subsequent TPS-internal translation from MD to SPR, usually done with a voxel-

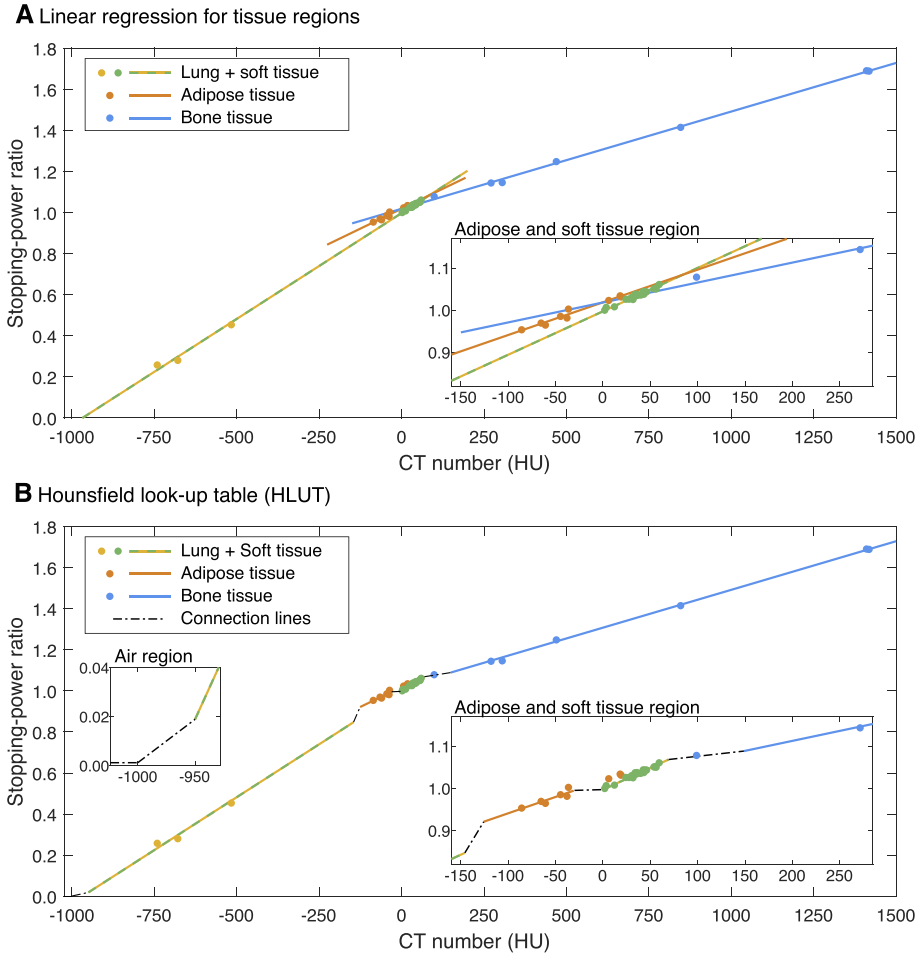

Fig. 1. (A) Individual datapoints and regression lines for the different tissue groups. **(B)** Generated Hounsfield look-up table (HLUT) with the regression lines limited to the tissue group-specific CT number interval and connection lines in-between. The two insets show the connection between neighbouring tissue groups. The slope is positive in each curve segment.

Table 1
CT scan and reconstruction parameters used for phantom scanning with CT scanners from GE HealthCare, Philips Healthcare and Siemens Healthineers. *Abbreviations*: SECT: single-energy CT; VMI: virtual monoenergetic CT image.

CT scanner	GE Revolution CT	Philips Spectral CT 7500	Siemens SOMATOM go.Open Pro
Tube voltage	120 kV	120 kV	120 kV
Scan mode	SECT	Spectral, 70 keV VMI	SECT
CTDI (32 cm / 16 cm)	20 mGy / 40 mGy	20 mGy / 40 mGy	20 mGy / 40 mGy
Field-of-view (body/head phantom)	500 mm / 250 mm	500 mm / 250 mm	500 mm / 250 mm
Rotation time	0.5 s	0.5 s	0.5 s
Pitch	0.52	0.8 (body) / 0.4 (head)	0.6
Detector collimation	64x0.625 mm	128x0.625 mm (body) / 064x0.625 mm (head)	64x0.6 mm
Slice thickness	2 mm	2 mm	2 mm
Slice increment	2 mm	2 mm	2 mm
Reconstruction kernel	Stnd, ASiR-V 50%	B (body) / UB (head)	Qr40, Admire 3, iBHC Bone

wise material assignment, cannot be configured by the user. While the recommendations were given specifically for proton and ion therapy, they can also be applied for photon therapy by using the calculated relative electron density instead of SPR.

In the most commonly used proton range prediction uncertainty estimation by Paganetti, the influence of the translation from CT numbers to SPR contributes more than 2% to the overall uncertainty of 3.5%, making it the dominating factor [2,6]. This estimation followed from the original work of Schaffner and Pedroni, where overall SPR prediction errors of 1.1% and 1.8% were assessed for the stoichiometric calibration in soft tissues and bones, respectively [20]. Similar uncertainty levels were described by Yang et al. [21], who comprehensively analysed the individual contributing factors. There, the influence of beam hardening as well as uncertainties in the stoichiometric calibration dominated. This was mitigated here by the recommendation of advanced beam hardening correction as well as the inclusion of both tabulated human tissues and tissue-equivalent phantom inserts in the HLUT specification. However, it should be noted that a potential improvement of range prediction following the application of the

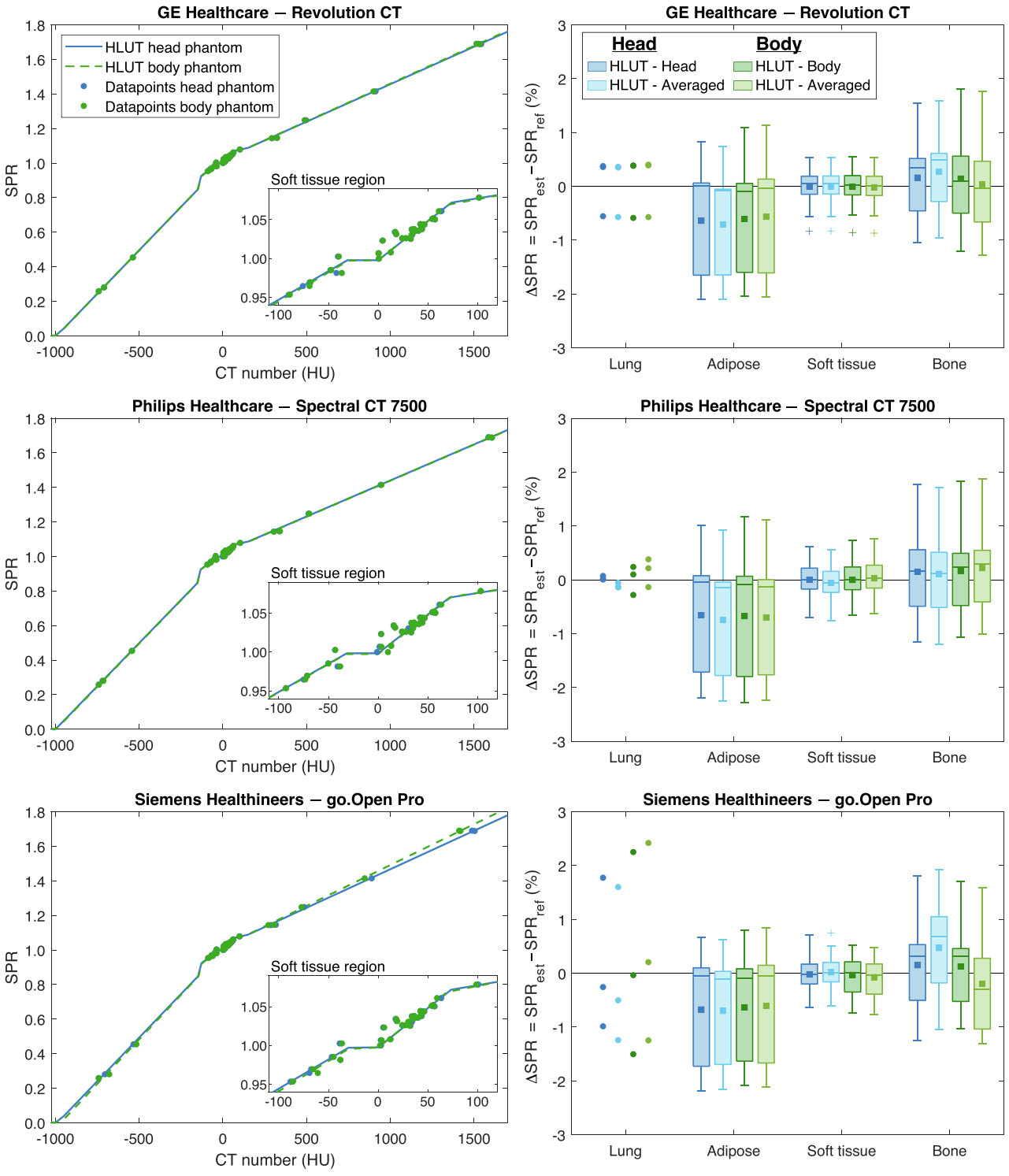

Fig. 2. (Left) Calibration datapoints (phantom inserts and tabulated human tissues) and the resulting HLUTs for the head and body phantom for three different CT scanners. **(Right)** SPR deviations of the calibration tissues in the head and body phantom from the respective HLUTs as well as from the HLUT for the averaged CT numbers, summarised in the respective tissue groups. For the boxplots, the boxes cover the interquartile range (25th to 75th percentile), the whiskers extend to 1.5 times the interquartile range, and outliers beyond this range are marked with a '+' symbol. The median and mean are indicated by the horizontal line and square within the box, respectively. Due to the limited number of datapoints, lung tissues are plotted individually.

presented guide heavily depends on the clinical scan setup and -protocol and can only follow from a comprehensive validation and uncertainty estimation of the centre-specific HLUT, as advised in Step 6.

The presented step-by-step guide focuses on SPR prediction for human tissues. Special care needs to be taken for non-tissue materials, such as bone cement, metals or silicone implants, which differ in composition from human tissues and are thus not considered in

the HLUT specification [22–25]. For voxels containing such materials, a manual material override of the SPR within the TPS is mostly inevitable. An exclusive consideration within the HLUT itself, e.g. by attributing CT numbers above a user-defined threshold to titanium could potentially result in an unintentional mis-assignment of dense tissues in some cases when using the HLUT.

A major limitation in accuracy of the SECT-based HLUT is its inability to handle the SPR variability for similar CT numbers observed in patients [26]. The use of DECT for a direct SPR prediction can overcome this limitation [27–32]; the resulting superior range prediction capability has been demonstrated in literature [33]. However, while several centres have access to a DECT scanner, only a fraction of the centres use it clinically [6,34]. Furthermore, the application of DECT is still limited, either to treatment areas without movement (e.g. head or pelvis), or to small body parts (e.g. head or extremities). Thus, only a subset of all cancer patients can currently be imaged with DECT. A consistent and precise SECT-based SPR estimation is therefore still indispensable.

The aim of the presented step-by-step guide, in combination with the exemplary implementation of the HLUT specification, was twofold: Increasing the accuracy in proton range prediction for treatment planning in individual proton centres and a lower inter-centre variation, enabling a better comparability of treatment data between different centres. At the same time, new imaging technologies such as DECT or magnetic resonance imaging for range prediction are pushing towards clinical application. To avoid a dilution of their clinical benefits due to uncertainties induced by non-standardised implementations across proton centres, similar guidance as highlighted here is desirable.

Declaration of Competing Interest

The authors declare that they have no known competing financial interests or personal relationships that could have appeared to influence the work reported in this paper.

Acknowledgment

We acknowledge grant funding from the National Cancer Institute NCI (R01 EB031102).

Appendix A. Supplementary material

Supplementary data to this article can be found online at https://doi.org/10.1016/j.radonc.2023.109675.

References

[1] Wohlfahrt P, Möhler C, Enghardt W, Krause M, Kunath D, Menkel S, et al. Refinement of the Hounsfield look-up table by retrospective application of patient-specific direct proton stopping-power prediction from dual-energy CT. Med Phys 2020;47:1796–806. https://doi.org/10.1002/mp.14085.
[2] Paganetti H. Range uncertainties in proton therapy and the role of Monte Carlo simulations. Phys Med Biol 2012;57:R99–R117. https://doi.org/10.1088/0031-9155/57/11/R99.
[3] Jäkel O, Jacob C, Schardt D, Karger CP, Hartmann GH. Relation between carbon ion ranges and X-ray CT numbers. Med Phys 2001;28:701–3. https://doi.org/10.1118/1.1357455.
[4] Schneider U, Pedroni E, Lomax A. The calibration of CT Hounsfield units for radiotherapy treatment planning. Phys Med Biol 1996;41:111–24. https://doi.org/10.1088/0031-9155/41/1/009.
[5] Witt M, Weber U, Kellner D, Engenhart-Cabillic R, Zink K. Optimization of the stopping-power-ratio to Hounsfield-value calibration curve in proton and heavy ion therapy. Z Med Phy 2015;25:251–63. https://doi.org/10.1016/j.zemedi.2014.11.001.
[6] Taasti VT, Bäumer C, Dahlgren CV, Deisher AJ, Ellerbrock M, Free J, et al. Inter-centre variability of CT-based stopping-power prediction in particle therapy: survey-based evaluation. Phys Imaging Radiat Oncol 2018;6:25–30. https://doi.org/10.1016/j.phro.2018.04.006.
[7] Peters N, Wohlfahrt P, Dahlgren CV, de Marzi L, Ellerbrock M, Fracchiolla F, et al. Experimental assessment of inter-centre variation in stopping-power and range prediction in particle therapy. Radiother Oncol 2021;163:7–13. https://doi.org/10.1016/j.radonc.2021.07.019.
[8] Woodard HQ, White DR. The composition of body tissues. Br J Radiol 1986;59:1209–18. https://doi.org/10.1259/0007-1285-59-708-1209.
[9] Wohlfahrt P. Dual-Energy Computed Tomography for Accurate Stopping-Power Prediction in Proton Treatment Planning. PhD Dissertation. Technische Universität Dresden, Dresden, Germany, 2018. https://nbn-resolving.org/urn:nbn:de:bsz:14-qucosa2-317554
[10] Fonseca GP, Baer-Beck M, Fournie E, Hofmann C, Rinaldi I, Ollers MC, et al. Evaluation of novel AI-based extended field-of-view CT reconstructions. Med Phys 2021;48:3583–94. https://doi.org/10.1002/mp.14937.
[11] Berger MJ, Inokuti M, Andersen HH, Bichsel H, Powers D, Seltzer SM, et al. ICRU report 49: stopping power and ranges for protons and alpha particles. J ICRU 1993:25. https://doi.org/10.1093/jicru/os25.2.Report49.
[12] Inaniwa T, Kanematsu N. Effective particle energies for stopping power calculation in radiotherapy treatment planning with protons and helium, carbon, and oxygen ions. Phys Med Biol 2016;61:N542–50. https://doi.org/10.1088/0031-9155/61/20/N542.
[13] Tattenberg S, Madden TM, Gorissen BL, Bortfeld T, Parodi K, Verburg J. Proton range uncertainty reduction benefits for skull base tumors in terms of normal tissue complication probability (NTCP) and healthy tissue doses. Med Phys 2021;48:5356–66. https://doi.org/10.1002/mp.15097.
[14] Tattenberg S, Madden TM, Bortfeld T, Parodi K, Verburg J. Range uncertainty reductions in proton therapy may lead to the feasibility of novel beam arrangements which improve organ-at-risk sparing. Med Phys 2022;49:4693–704. https://doi.org/10.1002/mp.15644.
[15] Hahn C, Eulitz J, Peters N, Wohlfahrt P, Enghardt W, Richter C, et al. Impact of range uncertainty on clinical distributions of linear energy transfer and biological effectiveness in proton therapy. Med Phys 2020;47:6151–62. https://doi.org/10.1002/mp.14560.
[16] Ainsley CG, Yeager CM. Practical considerations in the calibration of CT scanners for proton therapy. J Appl Clin Med Phys 2014;15:202–20. https://doi.org/10.1120/jacmp.v15i3.4721.
[17] Chacko MS, Wu D, Grewal HS, Sonnad JR. Impact of beam-hardening corrections on proton relative stopping power estimates from single- and dual-energy CT. J Appl Clin Med Phys 2022;23:e13711.
[18] Gomà C, Almeida IP, Verhaegen F. Revisiting the single-energy CT calibration for proton therapy treatment planning: a critical look at the stoichiometric method. Phys Med Biol 2018;63:. https://doi.org/10.1088/1361-6560/aaede5235011.
[19] Vergalasova I, McKenna M, Yue NJ, Reyhan M. Impact of computed tomography (CT) reconstruction kernels on radiotherapy dose calculation. J Appl Clin Med Phys 2020;21:178–86. https://doi.org/10.1002/acm2.12994.
[20] Schaffner B, Pedroni E. The precision of proton range calculations in proton radiotherapy treatment planning: experimental verification of the relation between CT-HU and proton stopping power. Phys Med Biol 1998;43:1579–92. https://doi.org/10.1088/0031-9155/43/6/016.
[21] Yang M, Zhu XR, Park PC, Titt U, Mohan R, Virshup G, et al. Comprehensive analysis of proton range uncertainties related to patient stopping-power-ratio estimation using the stoichiometric calibration. Phys Med Biol 2012;57:4095–115. https://doi.org/10.1088/0031-9155/57/13/4095.
[22] Lim YK, Hwang U-J, Shin D, Kim DW, Kwak J, Yoon M, et al. Proton Range Uncertainty Due to Bone Cement Injected Into the Vertebra in Radiation Therapy Planning. Med Dosim 2011;36:299–305. https://doi.org/10.1016/j.meddos.2010.05.005.
[23] Moyers MF, Mah D, Boyer SP, Chang C, Pankuch M. Use of proton beams with breast prostheses and tissue expanders. Med Dosim 2014;39:98–101. https://doi.org/10.1016/j.meddos.2013.10.006.
[24] Chacko MS, Grewal HS, Wu D, Sonnad JR. Accuracy of proton stopping power estimation of silicone breast implants with single and dual-energy CT calibration techniques. J Appl Clin Med Phys 2021;22:159–70. https://doi.org/10.1002/acm2.13358.
[25] Michalak G, Taasti V, Krauss B, Deisher A, Halaweish A, McCollough C. A comparison of relative proton stopping power measurements across patient size using dual- and single-energy CT. Acta Oncol 2017;56:1465–71. https://doi.org/10.1080/0284186X.2017.1372625.
[26] Wohlfahrt P, Möhler C, Troost EGC, Greilich S, Richter C. Dual-energy computed tomography to assess intra- and inter-patient tissue variability for proton treatment planning of patients with brain tumor. Int J Radiat Oncol Biol Phys 2019;105:504–13. https://doi.org/10.1016/j.ijrobp.2019.06.2529.
[27] Wohlfahrt P, Richter C. Status and innovations in pre-treatment CT imaging for proton therapy. Br J Radiol 2020;93:20190590. https://doi.org/10.1259/bjr.20190590.
[28] Hünemohr N, Krauss B, Tremmel C, Ackermann B, Jäkel O, Greilich S. Experimental verification of ion stopping power prediction from dual energy CT data in tissue surrogates. Phys Med Biol 2014;59:83–96. https://doi.org/10.1088/0031-9155/59/1/83.
[29] Wohlfahrt P, Möhler C, Richter C, Greilich S. Evaluation of stopping-power prediction by dual- and single-energy computed tomography in an anthropomorphic ground-truth phantom. Int J Radiat Oncol Biol Phys 2018;100:244–53. https://doi.org/10.1016/j.ijrobp.2017.09.025.
[30] Möhler C, Russ T, Wohlfahrt P, Elter A, Runz A, Richter C, et al. Experimental verification of stopping-power prediction from single- and dual-energy

computed tomography in biological tissues. Phys Med Biol 2018;63:. https://doi.org/10.1088/1361-6560/aaa1c9025001.
[31] Taasti VT, Michalak GJ, Hansen DC, Deisher AJ, Kruse JJ, Krauss B, et al. Validation of proton stopping power ratio estimation based on dual energy CT using fresh tissue samples. Phys Med Biol 2017;63:. https://doi.org/10.1088/1361-6560/aa952f015012.
[32] Paganetti H, Beltran C, Both S, Dong L, Flanz J, Furutani K, et al. Roadmap: proton therapy physics and biology. Phys Med Biol 2021;66:05RM01. https://doi.org/10.1088/1361-6560/abcd16.
[33] Peters N, Wohlfahrt P, Hofmann C, Möhler C, Menkel S, Tschiche M, et al. Reduction of clinical safety margins in proton therapy enabled by the clinical implementation of dual-energy CT for direct stopping-power prediction. Radiother Oncol 2022;166:71–8. https://doi.org/10.1016/j.radonc.2021.11.002.
[34] Hodgson KE, Larkin EA, Aznar MC, Vasquez OE. Dual-energy computed tomography: Survey results on current uses and barriers to further implementation. Br J Radiol 2021;94:20210565. https://doi.org/10.1259/bjr.20210565.